

Characterization and potential applications of new boron-phosphate glass in the $\text{CaO-P}_2\text{O}_5\text{-K}_2\text{O-B}_2\text{O}_3$ system

M. D. C. R. da Silva^{1*}, D. A. Bertuol¹, P. P. Lopes¹

¹Federal University of Santa Maria, Chemical Engineering Department, 97105-900, Santa Maria, RS, Brazil

Abstract

Boron phosphate glasses are known for their unique properties and have been investigated as biodegradable materials for biomedical applications. In this context, the present research studied the characterization of physical, mechanical, and bioactive properties of new boron-phosphate glass in the $\text{CaO-P}_2\text{O}_5\text{-K}_2\text{O-B}_2\text{O}_3$ system produced by the melt-quenching method. The structure and morphology of the material were investigated by FTIR, XRD, DSC, SEM-EDS, laser diffraction, and BET-BJH methods. Additionally, density and Vickers hardness were determined, and its bioactive potential was evaluated by immersion in simulated body fluid (SBF). The results demonstrated higher values of Vickers hardness (7.45 GPa) for the new glass when compared to other glasses. Furthermore, the material exhibited apatite-forming ability after immersion in SBF, which was confirmed by the information obtained through surface analysis. The newly created glass presented a promising potential for applications in tissue engineering.

Keywords: boron-phosphate, glasses, hardness, bioactivity, SEM.

INTRODUCTION

Materials for biomedical applications in tissue engineering have been researched in recent decades, aiming to produce improvements in the recovery process of affected tissues. Ceramic materials, especially glasses, play an important role in this field because of their unique properties [1]. Bioactive glasses have been studied due to their ability to form an apatite-like layer when in contact with body fluids (*in vivo* or *in vitro*). The first bioactive glass reported was the 45S5 in the early 1970s [2]. Bioactive silicate glasses have been widely studied after the development of the 45S5 glass [3]. However, these types of glasses remain in the organism for long periods after the bone cells grew. The released silicate species can easily polymerize and repolymerize to form new species with no resemblance to the original glass. Furthermore, the long-term effect of silica *in vivo* has not yet been explained [4].

Biodegradable and non-cytotoxic materials for hard tissue engineering applications are desirable because they are eventually replaced by natural tissue. In this scenario, phosphate glasses perform an important role. In terms of structure, phosphate glasses have a less strong network, leading to higher dissolution rates compared to silicate glasses [5]. Dissolution rates of this category of glasses can be controlled through their chemical composition. In addition, phosphate glasses have a chemical composition similar to bone, and several researches have revealed their bioactivity [5, 6]. The majority of glasses developed in recent years focused on the sol-gel process. This technique creates glasses with higher surface areas and porosity when

compared to the melt-quenched process, producing powders for applications with other materials (e.g., polymers) in scaffolds to improve mechanical and bioactivity properties. However, sol-gel glasses may have some disadvantages in terms of mechanical properties [3, 7]. Binary, ternary, and quaternary phosphate glasses have been developed over the last decades [8]. Most of them used Na_2O and CaO as modifiers, although other oxides, such as MgO , K_2O , and BaO , have been studied due to the improvements in their properties (e.g., bioactivity). Particularly, in the production of sintered bodies and coatings, the addition of K_2O can prevent crystallization during thermal treatments, which can improve glass bioactivity [9].

The boron-phosphate network presents unique characteristics for tissue engineering. Investigations showed that the addition of B_2O_3 to phosphate glasses improved their bioactivity by accelerating the formation of an apatite-like layer. Boron creates P-O-B crosslinks between the phosphate chains, improving mechanical, thermal, and physical properties [10]. Additionally, calcium ions can also promote crosslink formation between non-bridged oxygens of two different phosphate chains, strengthening the phosphate network [11]. Therefore, the simultaneous combination of CaO , K_2O , and B_2O_3 in a phosphate network can create a new formulation of glass that can present bioactive potential and better mechanical properties. In this scope, the study presented here aims to evaluate the structure, physical, mechanical, and bioactive properties of a new glass formulation in the system $\text{CaO-B}_2\text{O}_3\text{-K}_2\text{O-P}_2\text{O}_5$. Furthermore, glass powder characterization was investigated for biomedical applications.

EXPERIMENTAL

The reagents used in the preparation of the glass were

*eng.mauriciodallacosta@gmail.com

<https://orcid.org/0000-0002-7366-5316>

calcium phosphate monobasic monohydrate (Vetec, 95.0%), potassium phosphate dibasic trihydrate (Alphatec, 98.0%), and boric acid (Alphatec, 99.5%) as precursors of P_2O_5 , CaO, K_2O , and B_2O_3 . Chemical composition was determined by energy dispersive spectroscopy (EDS, VEGA3, Tescan) [12]. Glass compositions, nominal and experimental, are exhibited in Table I. The reagents (a total of 20 g) were homogenized using a mortar and pestle and then transferred to a crucible. The glass was prepared through the melt-quenching method in an electrically heated furnace at 1200 °C for 1.5 h with a heating rate of 10 °C/min in air. The frit was ground in a planetary ball mill (MA500, Marconi) for 60 min at 60 rpm of rotation and sieved with a 500 Tyler stainless steel screen in order to provide a powder with a size below 25 μm . The average particle size was determined by laser diffraction (mod. 1180, Cilas) in the range of 0.04 to 2500 μm . Glass samples were prepared for Vickers hardness and bioactivity tests. The process followed the method prior described, however, it was quenched in a steel plate and cooled to room temperature for 24 h. The samples were annealed in an electrically heated furnace at 600 °C for 60 min with a heating rate of 10 °C/min and cooled inside of the furnace until room temperature.

Table I - Composition (wt%) of boron-phosphate glass BV1 (experimental values in parenthesis).

CaO	P_2O_5	K_2O	B_2O_3
13.4 (12.86)	52.9 (55.23)	25.1 (25.04)	8.6 (6.87)

The material crystallinity was verified by X-ray diffraction (XRD, Miniflex 300, Rigaku) using monochromatic $\text{CuK}\alpha$ radiation generated at 30 kV and 10 mA, in the 2θ range of 5–65° with a resolution of 0.03°. The thermal behavior of the glass was determined by differential scanning calorimetry (DSC, DSC-60 Plus, Shimadzu) using an aluminum crucible at the range of 25–600 °C with 10 °C/min as the heating rate in a nitrogen atmosphere with a flow rate of 50 mL/min. By Fourier transform infrared spectroscopy (FTIR, IRPrestige-2, Shimadzu), the absorption spectrum was recorded at room temperature in the wavenumber range of 400–3900 cm^{-1} with a resolution of 2 cm^{-1} and 45 scans. The measurement was made by KBr pellet technique, using spectroscopic grade anhydrous KBr powder, pressed at 80 kN for 15 min. The pellet was dried for 60 min at 120 °C and cooled in a desiccator to remove the water excess. The glass density was determined by gas pycnometry with helium (Ultrapyc 1200, Quantachrome Instr.) in triplicate. Vickers hardness (HV) test was performed according to ASTM C1327-15 standard [13] using a microhardness tester (HMV-2, Shimadzu) with a square-based diamond pyramid indenter with 136° angle. Vickers hardness (GPa) was calculated by:

$$HV = 0.0018544 \left(\frac{P}{d^2} \right) \quad (\text{A})$$

where P is the applied force (N) and d is the average length of the two diagonals of the indentation (mm). Prior to indentation, the glass sample was polished with silicon carbide grinding papers P600 and P1200 to smooth the surface. Five indentations were made using 4.9 N of force applied for 15 s. Specific surface area, total pore volume, and average pore size of the powder were determined by nitrogen adsorption-desorption BET (Brunauer-Emmett-Teller) and BJH (Barrett-Joyner-Halenda) isotherms with an adsorption analyzer (ASAP 2020, Micromeritics). The powder was previously dried for 24 h in an air oven at 120 °C. The degassing conditions were: 10 °C/min rate, 30 °C target temperature, 1.0 mmHg/s evacuation rate, 15 μHg vacuum setpoint, and 100 mmHg hold pressure for 1 h in the evacuation step; and 10 °C/min rate, 100 mmHg hold pressure, and 150 °C hold temperature in the heating step.

Apatite-forming ability was investigated by immersion of the glass in a simulated body fluid (SBF) [14]. Sodium chloride (Alphatec, 99.5%), sodium bicarbonate (Neon, 99.5%), potassium chloride (Alphatec, 99.5%), potassium phosphate dibasic trihydrate (Alphatec, 98%), magnesium chloride hexahydrate (Alphatec, 98%), calcium chloride (Alphatec, 95%), sodium sulphate (Alphatec, 98%), TRIS (Biotecnologia, 98%), and 1.0 mol.L⁻¹ hydrochloric acid were used to prepare the SBF. The preparation of SBF followed the instructions described by Kokubo and Takadama [14]. In order to prepare 1000 mL of SBF, 700 mL of ultrapure water was first added into a 1000 mL plastic beaker under magnetic stirring and heating in a water bath until reaching 36.5±0.5 °C. At this temperature, the following reagents were dissolved one by one in the respective order and quantities: sodium chloride (8.035 g), sodium bicarbonate (0.355 g), potassium chloride (0.225 g), potassium phosphate dibasic trihydrate (0.231 g), magnesium chloride hexahydrate (0.311 g), 1.0 mol.L⁻¹ hydrochloric acid (39 mL), calcium chloride (0.292 g), and sodium sulfate (0.072 g). After dissolving the latter reagents, the solution volume (should be up to 900 mL; if not, ultrapure water was added to make up the volume) and pH (should be at 2.0±1.0) were verified before slowly dissolving 6.118 g of TRIS to raise the pH up to 7.45 at 36.5±0.5 °C. When pH had risen to 7.45±0.01, the dissolution of TRIS was stopped and 1.0 mol.L⁻¹ hydrochloric acid was carefully dropped using a syringe to lower the pH. When pH reached 7.42±0.01, the remaining TRIS was slowly dissolved until the pH had risen to 7.45. The pH for dissolving the remaining TRIS was kept within the range of 7.42–7.45 at 36.5±0.5 °C. After all, TRIS was solubilized, the pH was adjusted to 7.42±0.01 at 36.5±0.2 °C, and then to 7.40 exactly at 36.5 °C by adding 1.0 mol.L⁻¹ hydrochloric acid dropwise. The pH-

Table II - Ion concentrations (10⁻³ mol.L⁻¹) in SBF.

Na ⁺	K ⁺	Mg ²⁺	Ca ²⁺	Cl ⁻	HCO ₃ ⁻	HPO ₄ ²⁻	SO ₄ ²⁻
142.0	5.0	1.5	2.5	147.8	4.2	1.0	0.5

adjusted solution was transferred to a 1000 mL volumetric flask. The used beaker, stirring bar, and pH electrode were rinsed, the washings added to the flask, and ultrapure water was added. After mixing, the solution was cooled to 20 °C, and ultrapure water was added up to 1000 mL. Finally, the prepared SBF was stored in plastic bottles in a refrigerator. The ion concentrations of SBF are displayed in Table II.

Glass samples (5.3x4.2x3.2 mm) were soaked in SBF for 7, 14, and 28 days at 37 °C during the apatite-forming ability test. The volume of SBF used for testing was calculated according to Eq. B, proposed by Kokubo e Takadama [14], where V_s is the volume of SBF (mL) and S_a is the apparent surface area of the specimen (mm²). Morphological changes in the surface of the material were verified by scanning electron microscopy coupled with energy dispersive spectroscopy (SEM-EDS, VEGA3, Tescan).

$$V_s = \left(\frac{S_a}{10} \right) \quad (\text{B})$$

RESULTS AND DISCUSSION

The XRD patterns of BV1 powder and bulk samples are illustrated in Fig. 1. The diffractograms exhibited no sharp peaks thus revealing the absence of any crystalline phase and guaranteeing the amorphous nature of the material, characteristic of glasses. The thermal profile provided through DSC is illustrated in Fig. 2. The curve exhibited a baseline change in the range of 500-550 °C, characteristic of the glass transition. The temperature of glass transition (T_g) for the studied glass was 523 °C. No peaks were detected in the DSC curve, ensuring that the material was glass up to 600 °C. Moreover, the selected annealing temperature in this study (600 °C) was above the glass transition temperature, which provided minimization of the residual stress in glass samples and ensured material consistency. The XRD pattern of the BV1 bulk sample (Fig. 1) demonstrated that after annealing the material did not crystallize. This result could be assigned to the addition of K_2O , which was reported to prevent crystallization during thermal treatments [15].

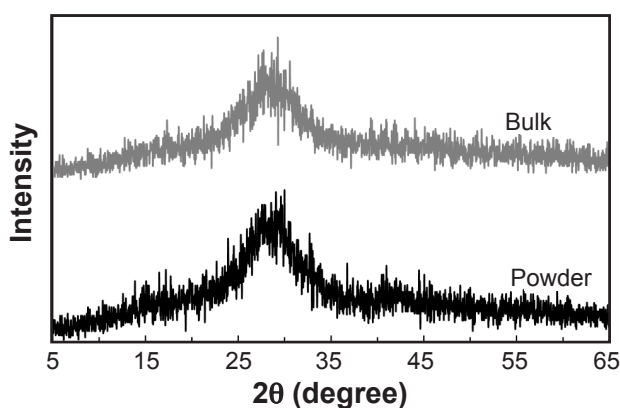


Figure 1: XRD patterns of powder and bulk samples of BV1 glass.

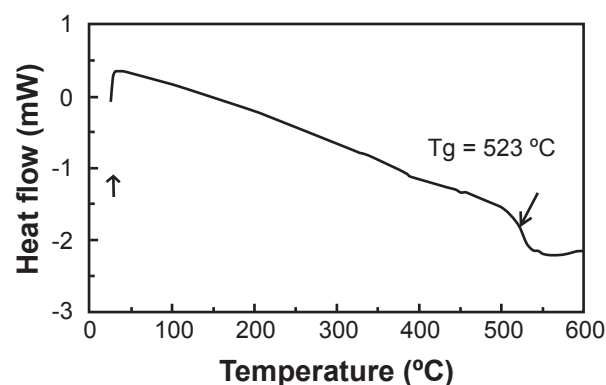


Figure 2: DSC curve of BV1 glass.

FTIR absorption spectroscopy was used to provide information about the arrangement of the phosphate and borate structural units in the glass network. The glass FTIR spectrum is displayed in Fig. 3. In the range between 400 and 1600 cm^{-1} , seven absorption bands located in regions near 547, 753, 912, 1039, 1111, 1166, and 1427 cm^{-1} were observed in the spectrum. In addition, in the range of 1600-3900 cm^{-1} , three main bands of absorption could be visualized at 3431, 2366, and 1647 cm^{-1} . The spectrum had the characteristic absorption bands of a phosphate-based glass mainly composed of pyrophosphate units (Q^2). In the range of 1600-3900 cm^{-1} , absorption bands related to the fundamental vibrations of the water and carbon dioxide molecules were present. The bands at 3431 and 1647 cm^{-1} were assigned to $\nu_s(\text{H-O-H})$ and $\delta(\text{H-O})$ vibrations of the water molecule, respectively, while the band at 2366 cm^{-1} was assigned to the $\nu_{as}(\text{CO})$ vibration of the carbon dioxide molecule [16]. The presence of water bands in the FTIR spectra is expected when the KBr pellet technique is used. Although the pellet was dried, phosphate glasses have a hygroscopic character and can absorb moisture from the air. The carbon dioxide absorption bands were due to the presence of small amounts of this gas in the compartment where the pellets were analyzed. Even though the equipment had a degassing system, some molecules might stay inside, absorbing a slight fraction of the beam energy. The absorption bands of phosphate and borate groups are located in the range 400-1600 cm^{-1} . The addition of B_2O_3 to the phosphate network creates an absorption band around 1400 and 1160 cm^{-1} . In Fig. 3, a band around 1427 cm^{-1} and a peak at 1166 cm^{-1} proved the presence of borate species in the glass structure [12]. The absorption peak at 1111 cm^{-1} can be explained by the $\nu_s(\text{O-P-O})$ vibration of Q^2 units on boron-phosphate-based glasses. The band at 1039 cm^{-1} can be assigned to P-O mode vibrations of terminal phosphate groups (Q^1) in glasses containing B_2O_3 and P_2O_5 as network formers [17]. The peak at 912 cm^{-1} was associated with $\delta_{as}(\text{P-O-P})$ vibrations in $K_2O\text{-CaO-P}_2\text{O}_5$ glasses [14] and the band at 753 cm^{-1} could be linked to $\nu_s(\text{P-O-P})$ vibration of the Q^2 units in boron-phosphate glasses [18, 19]. Finally, the peak at 540 cm^{-1} could be assigned to $\delta(\text{P-O-P})$ vibration modes on phosphate [20] and boron-phosphate [19] glasses with a slight shift in the wavenumber due to the presence of K_2O and CaO as modifiers.

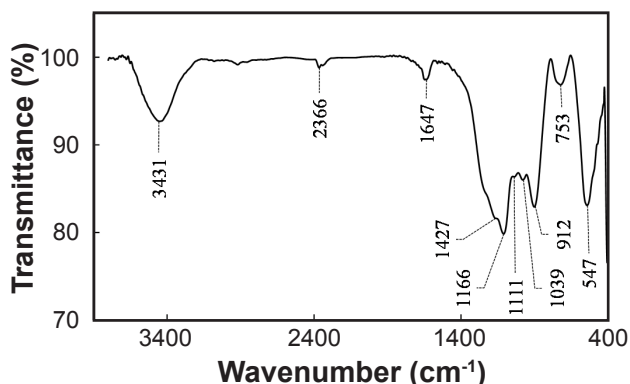


Figure 3: FTIR spectrum of BV1 glass.

The results of density and Vickers hardness are presented in Table III. Studies reported density values in the range of 2.39-2.56 g.cm⁻³ [21] and 2.30-2.47 g.cm⁻³ [22] in ternary boron-phosphate systems using Na₂O and K₂O as modifiers, respectively. The density value of BV1 glass (2.6066 g.cm⁻³) was above these values. This could be explained by the substitution of Na⁺ for K⁺ [9] and the addition of Ca²⁺ in the composition [23], which increased the density value due to higher atomic weight. Density varied between 2.62 and 2.77 g.cm⁻³ in boron-phosphate glasses containing BaO and Na₂O as modifiers [24], which can be associated with the higher atomic weight of Ba²⁺ and higher content of B₂O₃ in the composition. The addition of B₂O₃ in phosphate glasses can increase the number of cross-links due to the formation of B-O-P bridges [25]. Furthermore, Ca²⁺ ions can also promote reticulation in boron-phosphate networks [11, 26]. These could result in a more compact and rigid structure, leading to higher values of density and Vickers hardness when compared to some boron-phosphate glasses. The increase of B₂O₃ content from 5% to 30% improved the Vickers hardness from 4.599 to 6.175 GPa in boron-phosphate glasses [25]. Besides, values between 2.3 and 3.43 GPa were reported for Vickers hardness of boron-phosphate glasses with B₂O₃ content in the range of 0-20 mol% [24]. The addition of 6 mol% of B₂O₃ in glasses of the system P₂O₅-BaO-Al₂O₃-ZnO-Na₂O produced a material with 591.1 MPa of Vickers hardness value [27]. Also, the 45S5 bioactive glass was reported to have a Vickers hardness value of 3.78 GPa [28]. The material produced in this study had a higher value of Vickers hardness when compared to some of the later glasses. This could be associated with a more reticulated and rigid structure prior discussed.

Table III - Density and Vickers hardness of BV1 glass.

Density (g.cm ⁻³)	Vickers hardness (GPa)
2.6066±0.0003 (n=3)	7.45±0.30 (n=5)

Values of average particle size, BET surface area, average pore size, and total pore volume are presented in Table IV. The average pore size value obtained by the BJH desorption was between 2 and 50 nm, therefore suggesting

Table IV - BV1 powder characteristics.

Average particle size (μm)	BET surface area (m ² .g ⁻¹)	BJH desorption average pore size (nm)	BJH desorption total pore volume (cm ³ .g ⁻¹)
9.60	2.86	22.65	0.0129

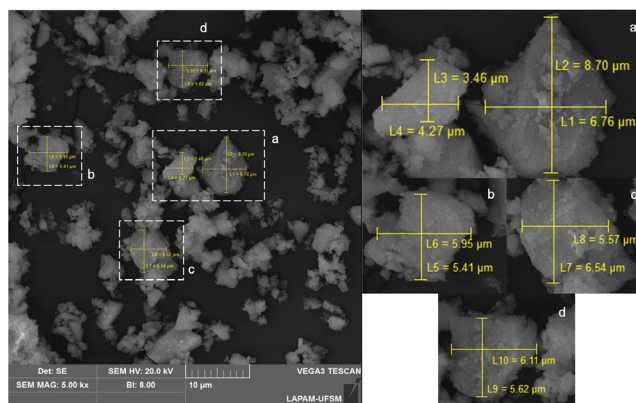


Figure 4: SEM micrographs of BV1 powder particles.

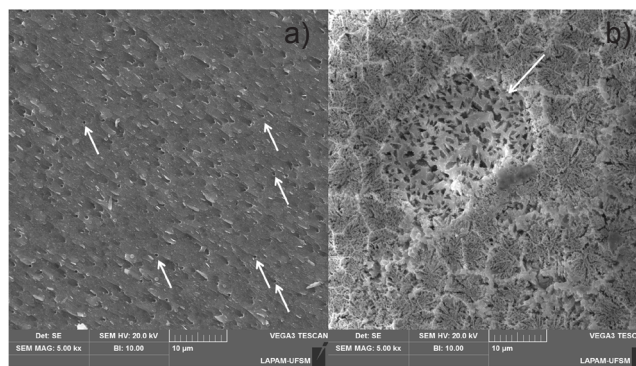


Figure 5: SEM micrographs of bulk BV1 surface before (a) and after 7 days of immersion in SBF (b).

the presence of mesoporous [29]. BET surface area and total pore volume values were 2.86 m².g⁻¹ and 0.0129 cm³.g⁻¹, respectively. The average particle size of 9.6 μm was in agreement with the dimensions exhibited in Fig. 4. Zinc-containing silicate glass particles and 45S5 glass particles with sizes below 26 μm were reported to have surface areas of 2 and 3 m².g⁻¹, respectively [30]. Additionally, glasses of the CaO-MgO-SiO₂ system with B₂O₃, Na₂O, CaF₂, and P₂O₅ additives presented surface area between 0.3 and 0.7 m².g⁻¹ for mean particle sizes of about 11-14 μm [31]. These results demonstrated that BV1 powder had a higher surface area compared to powders prior described and near to 45S5 powder with size below 26 μm. In addition, the immersion of the powder in a body fluid could increase its porosity and surface area due to the dissolution of the material [30]. The SEM images of the glass samples before and after 7 days of immersion in SBF (Fig. 5) were in accordance with this proposition.

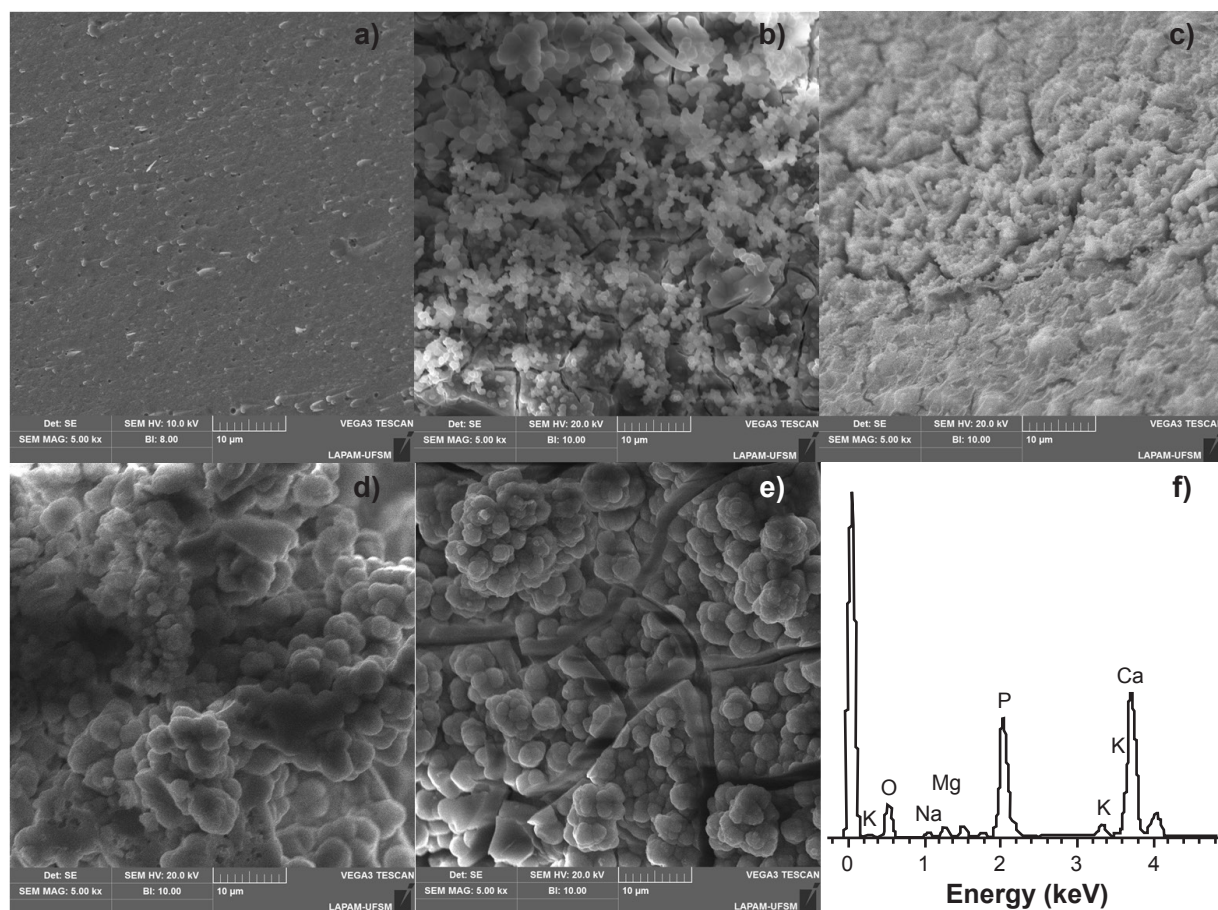


Figure 6: SEM micrographs of the BV1 glass surface before (a) and after 7 (b), 14 (c), 21 (d), and 28 (e) days of immersion in SBF and EDS spectrum after 28 days of immersion (f).

The SEM micrographs of the glass surface in the bioactive tests and the EDS spectrum are exposed in Fig. 6. Before soaking, the material surface was glassy and smooth without any deposits (Fig. 6a). After the immersion in SBF, modifications on the surface were detected. After 7 days, some spherical precipitates with different sizes were noticed (Fig. 6b). These precipitates could be assigned to apatite crystals due to their circular morphology. Usually, the precipitation of apatite crystal initiates with sole granules and then a dense layer develops on the surface of the material by the gradual growth of granules [28]. Similar results can be visualized on the surface as time progresses towards 14 days (Fig. 6c), 21 days (Fig. 6d), and 28 days (Fig. 6e) of immersion in SBF. The cracks in the subjacent layer became wider as the soaking time increased, which can be related to the biodegradation of the material due to diffusion and reactions between the glass surface and the SBF [32]. The EDS analysis was performed on the surface of the glass after immersion in SBF for 28 days (Fig. 6f). The results showed the presence of spherical particles on the surface with a Ca/P atomic ratio of 1.40, indicating the presence of a calcium-deficient (non-stoichiometric) hydroxyapatite [33], which is supposed to be bioactive and more similar to natural bone minerals with regard to chemical composition and crystal structure [34]. This type of apatite formed on the surface of

a biomaterial after immersion in SBF indicates its possible *in vivo* biological activity. These results demonstrated that BV1 glass has a potential of apatite-like layer formation on its surface, contributing to its ability to bone bonding with living tissues.

CONCLUSIONS

A new glass (called BV1) in the CaO-P₂O₅-K₂O-B₂O₃ system was successfully prepared through the melt-quenching method. The addition of K₂O prevented crystallization of the material after annealing at 600 °C, which was confirmed by XRD analysis. DSC thermal profile exhibited the glass transition temperature and absence of crystallization and melting temperatures up to 600 °C, thus confirming that the material produced was glass. FTIR spectrum showed the characteristic absorption bands of a boron-phosphate glass. The addition of B₂O₃ together with CaO in the formulation provided structure rigidity and compactness, improving the mechanical properties, which could be confirmed by the values of Vickers hardness: BV1 presented higher values of Vickers hardness when compared to other boron-phosphate and silicate glasses. The density values also reflected the network features. BJH results suggested that BV1 powder particles were composed of mesopores. The values of the

BET surface area proved to be higher than some fine silicate-based glass powders with similar granulometry. SEM micrographs of the surface during the *in vitro* evaluation of apatite-forming ability showed the deposition of spherical precipitates, characteristic of apatite crystals. They grew as the immersion time in SBF progressed along with cracks in the subjacent layer, which indicated the dissolution of BV1. After 28 days of immersion, EDS analysis demonstrated the presence of deposits of calcium-deficient (non-stoichiometric) hydroxyapatite on the surface, indicating its bioactive potential. This material has promising applications in tissue engineering due to its mechanical and bioactive properties, however further studies are needed to evaluate its *in vivo* biocompatibility and other properties.

ACKNOWLEDGMENTS

The authors acknowledge the Coordination for the Improvement of Higher Education Personnel (CAPES) for financial support and the Environmental Processes Laboratory (LAPAM) at the Federal University of Santa Maria for technical support.

REFERENCES

- [1] V.J. Shirliff, L.L. Hench, *J. Mater. Sci.* **38** (2003) 4697.
 - [2] L.L. Hench, *J. Am. Ceram. Soc.* **81**, 7 (1998) 1705.
 - [3] G. Kaur, G. Pickrell, N. Sriranganathan, V. Kumar, D. Homa, *J. Biomed. Mater. Res. B Appl. Biomater.* **140**, 6 (2016) 1248.
 - [4] N. Sharmin, C.D. Rudd, *J. Mater. Sci.* **52** (2017) 8733.
 - [5] E.A. Abou Neel, D.M. Pickup, S.P. Valappil, R.J. Newport, J.C. Knowles, *J. Mater. Chem.* **19** (2009) 690.
 - [6] I. Ahmed, M. Lewis, I. Olsen, J.C. Knowles, *Biomaterials* **25** (2004) 491.
 - [7] G. Kaur, V. Kumar, F. Baino, J.C. Mauro, G. Pickrell, I. Evans, O. Breteanu, *Mater. Sci. Eng. C* **104** (2019) 109895.
 - [8] J.C. Knowles, *J. Mater. Chem.* **13** (2003) 2395.
 - [9] S.M. Rabiee, N. Nazparvar, M. Azizian, D. Vashae, L. Tayebi, *Ceram. Int.* **41** (2015) 7241.
 - [10] J. Massera, Y. Shpotyuk, F. Sabatier, T. Jouan, C. Boussard-Plédel, C. Roiland, B. Bureau, L. Petit, N.G. Boetti, D. Milanese, L. Hupa, *J. Non-Cryst. Solids* **425** (2015) 52.
 - [11] N. Sharmin, C.D. Rudd, A.J. Parsons, I. Ahmed, *J. Mater. Sci.* **51** (2016) 7523.
 - [12] A. Saranti, I. Koutselas, M.A. Karakassides, *J. Non-Cryst. Solids* **352** (2006) 390.
 - [13] C1327-15, “Standard test method for Vickers indentation hardness of advanced ceramics”, ASTM Int., West Conshohocken (2019).
 - [14] T. Kokubo, H. Takadama, *Biomaterials* **27** (2006) 2907.
 - [15] V. Cannillo, A. Sola, *Ceram. Int.* **35** (2009) 3389.
 - [16] R.M. Silverstein, F.X. Webster, *Spectrometric identification of organic compounds*, Wiley, New York (1998).
 - [17] D. Carta, D. Qiu, P. Guerry, I. Ahmed, E.A. Aboul Neel, J.C. Knowles, M.E. Smith, R.J. Newport, *J. Non-Cryst. Solids* **354** (2008) 3671.
 - [18] A.N. Regos, R.C. Lucacel, I. Ardelean, *J. Mater. Sci.* **46** (2011) 7313.
 - [19] I.J. Hidi, G. Melinte, R. Stefan, M. Bindea, L. Baia, *J. Raman Spectrosc.* **44** (2013) 1187.
 - [20] L. Baia, D. Muresan, M. Baia, J. Popp, S. Simon, *Vib. Spectrosc.* **43** (2007) 313.
 - [21] D. Zielniok, C. Cramer, H. Eckert, *Chem. Mater.* **19** (2007) 3162.
 - [22] D. Larink, H. Eckert, M. Reichert, S.W. Martin, *J. Phys. Chem. C* **116** (2012) 26162.
 - [23] A.A. Ahmed, A.A. Ali, A. El-Fiqi, *J. Mater. Res. Technol.* **8**, 1 (2019) 1003.
 - [24] K.V. Shah, M. Goswami, M.N. Deo, A. Sarkar, S. Manikandan, V.K. Shrikhande, G.P. Kothiyal, *Bull. Mater. Sci.* **29**, 1 (2006) 43.
 - [25] S.M. Abo-Naf, E.S.M. Khalil, E.S.M. El-Sayed, H.A. Zayed, R.A. Youness, *Spectrochim. Acta A Mol. Biomol. Spectrosc.* **144** (2015) 88.
 - [26] N.H. Youssef, M.S. Belkhiria, J.J. Videau, M. Ben Amara, *Mater. Lett.* **44** (2000) 269.
 - [27] Y. Zhao, Y. Zhou, J. Yang, Y. Li, L. Cheng, K. Wang, X. Sun, C. Sun, Z. Qin, *Ceram. Int.* **46** (2020) 9025.
 - [28] B. Karakuzu-İkizler, P. Terzioğlu, B.S. Oduncu-Tekerek, S. Yücel, *J. Aust. Ceram. Soc.* **56** (2020) 697.
 - [29] M. Thommes, K. Kaneko, A.V. Neimark, J.P. Olivier, F. Rodriguez-Reinoso, J. Rouquerol, K.S.W. Sing, *Pure Appl. Chem.* **87**, 9-10 (2015) 1051.
 - [30] V. Aina, G. Malavasi, A. Fiorio Pla, L. Munaron, C. Morterra, *Acta Biomater.* **5**, 4 (2009) 1211.
 - [31] S. Agathopoulos, D.U. Tulyaganov, J.M.G. Ventura, S. Kannan, M.A. Karakassides, J.M.F. Ferreira, *Biomaterials* **27** (2006) 1832.
 - [32] Y.W. Gu, K.A. Khor, P. Cheang, *Biomaterials* **24** (2006) 1603.
 - [33] J.D. Masson, M. Thibaudon, L. Bélec, G. Crépeaux, *Expert Rev. Vaccines* **16**, 3 (2017) 289.
 - [34] X. Li, Y. Deng, M. Wang, X. Chen, Y. Xiao, X. Zhang, *J. Mater. Chem. B* **6** (2018) 84.
- (*Rec. 26/08/2021, Rev. 07/10/2021, Ac. 11/10/2021*)